Study of the effect of energy window width and peak shift on SPECT images to evaluate false diagnosis

Original Article

Mahidul Haque Prodhan[1], Hasan Talukder[2], Fazlul Huq[1], Zahid Hasan Mahmood[2]

[1]Department of Nuclear Engineering, University of Dhaka, Dhaka, Bangladesh
[2]Department of Electrical and Electronic Engineering, University of Dhaka, Dhaka, Bangladesh

(Received 8 May 2015, Revised 9 December 2015, Accepted 20 December 2015)

ABSTRACT

Introduction: The different factors that affect the camera uniformity of Single Photon Emission Computed Tomography (SPECT) technique have been analyzed including peak shift (%) and window width of energy. The effect of peak shift and window width on SPECT image uniformity has been investigated using a point source to perform intrinsic flood images.

Methods: The relation between calculated integral & differential Center Field of View (CFOV) and Useful Field of View (UFOV) uniformity values were plotted with peak shift and window width change. The effects of window width of energy 5%, 10%, 15%, 20% and 25% on SPECT images were investigated using the ^{99m}Tc radioisotope with energy of 140 keV.

Results: Although 0% shift is the optimum peak shift, but in the current research we have found that the data in the range of 0% to 2% peak shift provides result with satisfactory image quality. Integral Uniformity (IU %) and Differential Uniformity (DU %) values of CFOV and UFOV were noticeably changed with the change of energy window width. In this research, the optimum energy window width of the images of different flood phantom has been found to be in the range from 15% to 20%.

Conclusion: Finally, 0% to 2% peak shift at 15% energy window width applied on heart phantom provides suitable images leading to proper diagnosis which conform our findings.

Key words: SPECT; Center field of view (CFOV); Useful field of view (UFOV); Integral uniformity (IU); Differential uniformity (DU)

Iran J Nucl Med 2016;24(2):76-84
Published: July, 2016
http://irjnm.tums.ac.ir

Corresponding author: Md. Mahidul Haque Prodhan, Department of Nuclear Engineering, University of Dhaka, Dhaka – 1000, Bangladesh. E-mail: mahiapecedu@gmail.com

INTRODUCTION

Nuclear imaging techniques involve the use of scintillation Gamma cameras for diagnostic imaging of the lung, brain, thyroid, heart, liver etc. with topographic facilities connected to computer systems [1]. Baron *et al*. has reported the need to ensure consistently high image quality and accuracy using an optimally chosen standardized protocol [2]. It has been reported that SPECT significantly improves contrast over the planer image and has the ability to separate overlapping structures [3-5].

Single Photon Emission Computed Tomography (SPECT) and Positron Emission Tomography (PET) techniques are utilized to perform such diagnostic imaging. SPECT imaging is preferred to planar imaging for situations involving organs with complex 3D geometry or structure, such as the brain and heart, and for tumor localization and characterization [6,7]. SPECT, using a rotating gamma camera, needs accurate calibration of the electromechanical components, detection system and reconstruction software [8-10].

SPECT imaging uses the same radiotracers labeled with single γ-emission radionuclides and, to a large extent, the same imaging instruments as conventional nuclear medicine imaging. Hence, the wide variety of radio-pharmaceuticals, most labeled with ^{99m}Tc, can be used to gather 3D information on the in vivo function [11, 12] of tissues and organs non-invasively [6, 13].

Performance measurements of gamma camera and other tests include pixel size calibration, linearity measurements, rotational sensitivity, mechanical alignment, energy distribution and counting rate capabilities [3, 4]. However, the most sensitive indicator of gamma camera performance is uniformity as it is performed on a daily basis as well as being the principle tool in evaluating the status of the camera. Most artifacts related to the integrity of the detector head, computer system and hard-copy device can be detected on the uniformity image. Ring or band artifacts are caused by a variety of factors influencing the counting accuracy of a detector, such as gain variations, radiation damage to the detector, and linearity irregularities. Ring artifacts can be very frustrating at times. Root cause is non-uniformity. Small non-uniformity can cause ring artifacts. So, if artifacts are not present on a High Quality SPECT acquisition then that will assure, SPECT uniformity is good.

The common sources of artifacts are non-uniformity in gamma-camera detectors, center of rotation errors, misaligned cameras on multi-detector [14] scanner systems, errors in image reconstruction, patient motion and radiotracer uptake in non-target organs and attenuation. The best way to avoid these artifacts is to pay very close attention to the technical factors of image acquisition, as well as processing away from attenuation factors [15]. The effects of center-of-rotation (COR) shift on contrast and spatial resolution of SPECT systems [16], and shift of rotating camera-based SPECT system on the tomography of images [17, 18] have already been reported.

Two types of uniformity parameters are considered in SPECT imaging. Among them, the Integral Uniformity (IU) is calculated as [19],

$$IU\ (\%) = \pm 100\,\% \times \frac{Max - Min}{Max + Min} \qquad (1)$$

The maximum and the minimum pixel counts are found from the smoothed data. On the other hand, the Differential Uniformity (DU) is calculated as [20],

$$DU\ (\%) = \pm 100\,\% \times \frac{High - Low}{High + Low} \qquad (2)$$

The calculation is done for the X and the Y directions independently.

The Uniformity of SPECT images, both differential and integral, changes with the change in peak shift and window width.

In this research, the effects of window width of energy 5%, 10%, 15%, 20% & 25% and peak shift of 0%, 1%, 2%, 3%, 4% & 5% on SPECT images have been investigated using intrinsic flood images and extrinsic phantom flood images. Hence it is seen that the optimum energy window width of the images of different flood phantom has been found to be in the range from 15% to 20% with 0% to 2% peak shift.

METHODS

Source materials and scanner

The radionuclide used to measure intrinsic uniformity is ^{99m}Tc (activity between 20-30 μCi). The gamma camera used in this study was a dual head variable angle system, model E. Cam Series manufactured by Siemens (Model No.7823946).

System uniformity matrix

The crucial factor, beside the quality of the acquired images, is the system matrix. Each element gives the probability of detecting the photon emitted from the image in the detector. The basis of the system matrix construction is gamma camera geometry. It depends on the field of view of the detector point. Assuming ideal collimation of the beam, this matrix can be determined using a ray-based or a pixel-based approach. An alternative to the analytical methods mentioned is to compute the system matrix using Monte Carlo simulations. We used the matrix size to a maximum available value of 1024× 1024.

Test conditions

In the current research, the total count has been taken 10,000 kcts through all of symmetric 5%, 10%, 15%, 20% & 25% photo peak window width.

Data collection

Data for 0%, 1%, 2%, 3%, 4% and 5% peak shift and the uniformity values of integral and differential CFOV & UFOV for window width of 5%, 10%, 15%, 20% and 25% has been obtained. The corresponding relation between peak shift and CFOV & UFOV uniformity values has been plotted. It is to be noted that the data were collected from separate computer with the help of medical software (Syngo: SyngoMI VA40B).

Phantom studies

The effect of peak shift on SPECT images has also been studied using the heart phantom. This study consisted of using the heart phantom in multi-SPECT acquisition for different peak shifts (2%, 4% and 6%) at window width of 15% using the same parameters in each acquisition. The acquisition parameter has also been shown in the Table 1.

Table 1: Acquisition parameters

Parameter	Value
Matrix size	1024×1024
Magnification	1
Count rate	10 K counts/s
Rotation type	Step & shoot
Orbit type	Body contour
No. of views per scan	32
Detector configuration	90°

RESULTS AND DISCUSSION

Effect of peak shift on uniformity

In Figure 1a, clear distinction between hot and cold areas i.e. bright and dark spots, present an evidence of the decrease in uniformity with increasing the peak shift percentage.

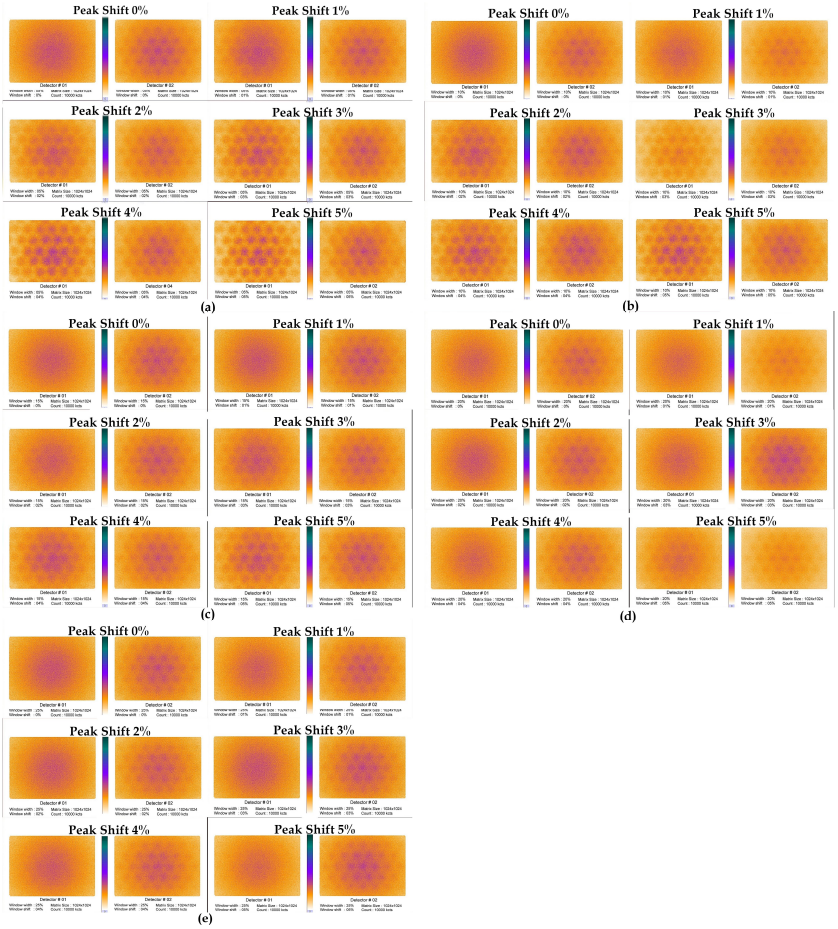

Fig 1. Flood images for different peak shift percentage at window width of (a) 5% (b) 10% (c) 15% (d) 20% (e) 25%.

There is a discrepancy between hot and cold areas, shown in Figure 1b offering strong indication on the decrease in uniformity with the increasing of the peak shift percentage. That the quality of the image becomes bad.

In Figure 1c, hot and cold areas i.e. bright and dark spots, offer a confirmation of little decrease in uniformity with increasing the peak shift percentage. Here, differentiation between hot and cold areas is not clearly visualized in the peak shift range from 0 to 2%, while in the peak shift range of more than 2% the quality of the image becomes worse, so the change in the image is clearly observed.

There exists an inconsistency in between hot and cold areas, as shown in Figure 1d, which is an evidence of decrease in uniformity with increasing peak shift percentage.

It can also be shown that the differentiation between hot and cold areas is not clearly visualized in the peak shift range from 0 to 2%, while in the peak shift range of more than 2% the quality of the image becomes worse, so the change in the image is evident.

From Figure 1e, a disparity between hot and cold areas gives a confirmation of the decrease in uniformity with increasing the peak shift percentage.

At window width of 5%: Based on data obtained from the experiment as shown in Table 2, a noticeable increase in the calculated values of the uniformity in the peak shift range from 0 to 5% is evident. Figure 2a clearly shows that the value of uniformity linearly increases with increase in peak shift that refers loss of uniformity.

According to the data on Table 3, there is also an increase in the values of uniformity in the peak shift range from 0 to 5%, which is also evident from Figure 2b.

Table 2: The calculated values of integral and differential uniformities in CFOV & UFOV for 0%, 1%, 2%, 3%, 4% & 5% peak shift at window width of 5% (Detector 1).

Detector -1				
Peak Shift	**Integ. CFOV**	**Diff. CFOV**	**Integ. UFOV**	**Diff. UFOV**
0 %	4.97%	3.13%	4.97%	3.10%
1 %	7.32%	5.85%	9.79%	7.47%
2 %	12.99%	10.29%	16.45%	11.23%
3 %	17.64%	13.71%	21.06%	15.84%
4 %	23.06%	17.80%	27.01%	18.17%
5 %	27.80%	22.67%	34.55%	23.08%

Table 3: The calculated values of integral and differential uniformities in CFOV & UFOV for 0%, 1%, 2%, 3%, 4% & 5% peak shift at window width of 5% (Detector 2).

Detector -2				
Peak Shift	**Integ. CFOV**	**Diff. CFOV**	**Integ. UFOV**	**Diff. UFOV**
0 %	8.58%	6.29%	9.30%	6.29%
1 %	8.96%	6.44%	9.53%	6.44%
2 %	9.62%	6.49%	12.80%	6.99%
3 %	11.21%	7.64%	14.76%	9.42%
4 %	13.07%	8.24%	16.19%	9.88%
5 %	14.59%	9.74%	19.13%	12.40%

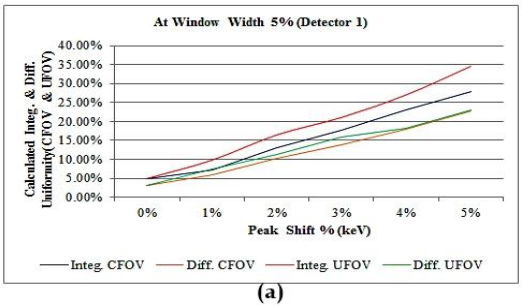

(a)

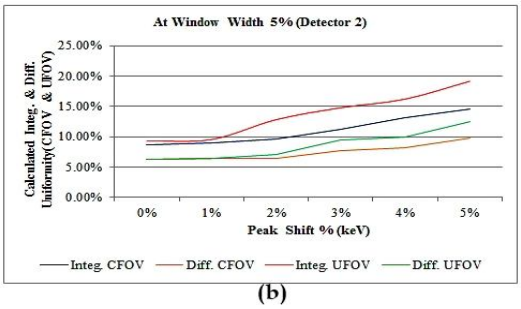

(b)

Fig 2. The calculated integral and differential uniformities in CFOV & UFOV (arbitrary units) versus peak shift percentage (keV) at window width of 5% ((a) Detector 1 and (b) Detector 2).

At window width of 10%: In Figure 3a, Also increase in values (based on Table 4) of uniformity in the peak shift range from 0 to 5% can be easily noted, representing a loss of uniformity.

A small increase in the calculated values according (shown in Table 5) of the uniformity in the peak shift range from 0 to 2% can be easily noted in Figure 3b representing a loss of uniformity. In the peak shift range from 3 to 5%, a decrease & a rapid increase in the integral & differential values in both fields (CFOV & UFOV), which indicates an instability in uniformity.

Table 4: The calculated values of integral and differential uniformities in CFOV & UFOV for 0,1,2,3, 4 & 5% peak shift at window width of 10% (Detector 1).

Detector -1				
Peak Shift	**Integ. CFOV**	**Diff. CFOV**	**Integ. UFOV**	**Diff. UFOV**
0 %	4.69%	1.91%	5.19%	2.63%
1 %	5.89%	4.12%	6.50%	4.41%
2 %	12.47%	10.01%	14.69%	11.30%
3 %	15.88%	12.63%	19.85%	14.40%
4 %	17.50%	14.26%	19.58%	14.26%
5 %	21.18%	16.36%	24.15%	17.09%

Table 5: The calculated values of integral and differential uniformities in CFOV & UFOV for 0,1,2,3, 4 & 5% peak shift at window width of 10% (Detector 2).

Detector -2				
Peak Shift	**Integ. CFOV**	**Diff. CFOV**	**Integ. UFOV**	**Diff. UFOV**
0 %	8.43%	6.67%	8.95%	6.67%
1 %	8.73%	6.52%	9.55%	6.52%
2 %	8.85%	5.90%	10.23%	6.15%
3 %	9.42%	5.89%	11.46%	6.90%
4 %	10.46%	7.07%	15.07%	8.33%
5 %	11.81%	7.73%	15.77%	8.89%

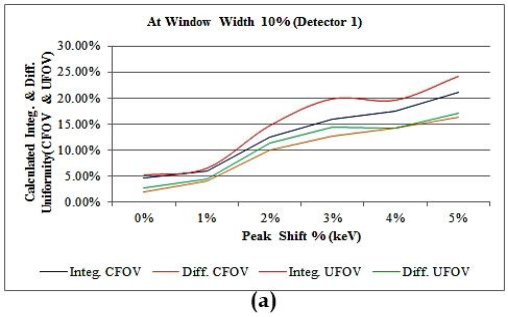

(a)

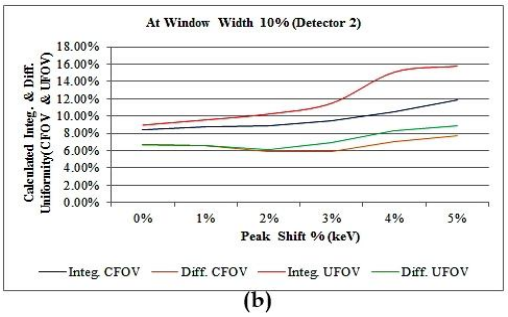

(b)

Fig 3. The calculated integral and differential uniformities in CFOV & UFOV (arbitrary units) versus peak shift percentage (keV) at window width of 10% ((a) Detector 1& (b) Detector 2).

At window width of 15%: The calculated values found from Table 6, very little increase both integral and differential uniformities in the peak shift range from 0 to 2%, can be noticed. Figure 4a shows a very little loss in uniformity. In the range from 3 to 4%, an increase in the calculated values giving more loss in both uniformities. In the range from 3 to 4%, the graph shows a flat curve, however, it indicates loss in the uniformity. A very small increase in the calculated values (as shown in Table 7) in both integral and differential uniformities can be noticed in Figure 4b in the peak shift range from 0% to 2%, indicating a little loss in uniformity. In the range from 3% to 4%, the graph shows a flat curve, representing little loss in the uniformity. The values of uniformity increases rapidly in the range of more than 4% peak shift, which means that the uniformity becomes worse.

Table 6: The calculated values of integral and differential uniformities in CFOV & UFOV for 0,1,2,3, 4 and 5% peak shift at window width of 15% (Detector 1).

Detector -1				
Peak Shift	**Integ. CFOV**	**Diff. CFOV**	**Integ. UFOV**	**Diff. UFOV**
0 %	4.32%	2.17%	4.72%	2.65%
1 %	4.54%	2.37%	5.13%	2.79%
2 %	5.81%	4.72%	6.67%	4.72%
3 %	8.32%	6.88%	8.76%	6.88%
4 %	10.43%	7.53%	11.01%	8.44%
5 %	12.79%	9.90%	14.73%	10.24%

Table 7: The calculated values of integral and differential uniformities in CFOV & UFOV for 0,1,2,3, 4 and 5% peak shift at window width of 15% (Detector 2).

Detector -2				
Peak Shift	**Integ. CFOV**	**Diff. CFOV**	**Integ. UFOV**	**Diff. UFOV**
0 %	8.22%	5.42%	8.67%	5.72%
1 %	8.22%	5.28%	8.96%	5.26%
2 %	8.96%	5.53%	9.92%	5.87%
3 %	8.16%	6.19%	9.88%	6.17%
4 %	8.96%	6.06%	10.94%	6.37%
5 %	9.90%	6.25%	12.39%	8.27%

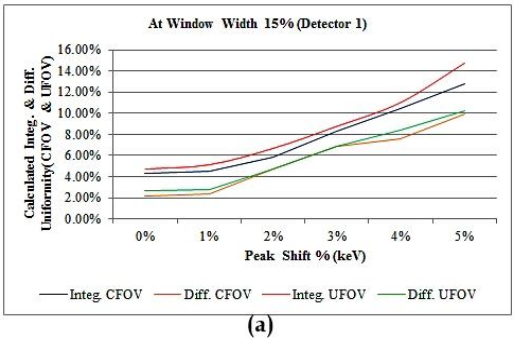

(a)

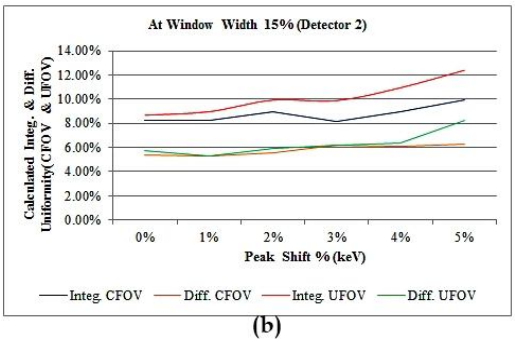

(b)

Fig 4. The calculated integral and differential uniformities in CFOV & UFOV (arbitrary units) versus peak shift percentage (keV) at window width of 15% ((a) Detector 1& (b) Detector 2).

At window width of 20%: In the peak shift range from 0 to 3%, a small decrease in the calculated values found from Table 8, indicating good uniformity as pointed out in Figure 5a. But a small increase in the calculated uniformity values in the range from 2 to 3%, giving bad uniformity. Also, in the range from 3 to 4%, Figure shows more loss in the uniformity.

In Figure 5b, a small increase in the calculated values in both integral and differential uniformities can be noticed in the peak shift range from 0 to 2%, giving a little loss in uniformity which is also evident in Table 9. In the range of 2 to 4%, the graph shows a flat curve, however, it indicates more loss in the uniformity.

Table 8: The calculated values of integral and differential uniformities in CFOV & UFOV for 0, 1, 2, 3, 4 and 5% peak shift at window width of 20% (Detector 1).

Detector -1				
Peak Shift	**Integ. CFOV**	**Diff. CFOV**	**Integ. UFOV**	**Diff. UFOV**
0 %	4.46%	2.29%	4.74%	2.64%
1 %	4.39%	2.05%	4.97%	2.54%
2 %	4.31%	2.33%	5.91%	3.76%
3 %	4.34%	3.01%	5.20%	3.78%
4 %	6.10%	4.05%	7.11%	4.97%
5 %	7.83%	5.81%	8.17%	6.73%

Table 9: The calculated values of integral and differential uniformities in CFOV & UFOV for 0, 1, 2, 3, 4 and 5% peak shift at window width of 20% (Detector 2).

Detector -2				
Peak Shift	**Integ. CFOV**	**Diff. CFOV**	**Integ. UFOV**	**Diff. UFOV**
0 %	8.57%	5.27%	8.96%	5.35%
1 %	8.05%	5.56%	9.52%	5.51%
2 %	8.15%	5.59%	8.36%	5.52%
3 %	8.43%	5.50%	9.71%	5.50%
4 %	8.90%	5.68%	9.68%	6.23%
5 %	8.51%	5.51%	9.80%	6.31%

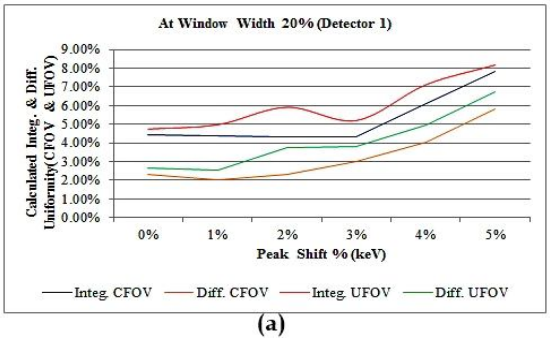

(a)

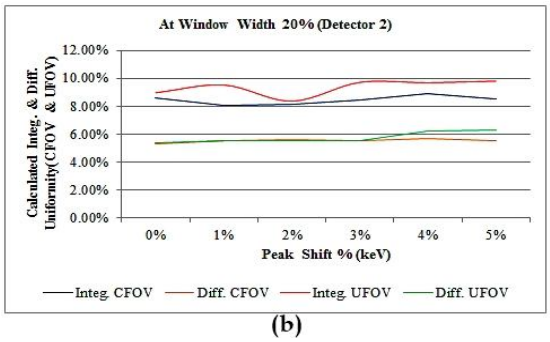

(b)

Fig 5. The calculated integral and differential uniformities in CFOV & UFOV (arbitrary units) versus peak shift percentage (keV) at window width of 20% ((a) Detector 1& (b) Detector 2).

At window width of 25%: From Table 10 it is evident that, a little increase in the calculated values of the uniformity in the peak shift range from 0 to 3% can be easily noted, indicating a little loss of uniformity (Figure 6a). In the range from 4 to 5%, there is a rapid increase in the differential & integral values in both fields, CFOV and UFOV. Hence, a noticeable loss of uniformity is to be observed.

In Figure 6b a little increase in the calculated values (Table 11) of the uniformity in the peak shift range from 0 to 5% can be easily noted, indicating a loss of uniformity.

Table 10: The calculated values of integral and differential uniformities in CFOV & UFOV for 0, 1, 2, 3, 4 and 5% peak shift at window width of 25% (Detector 1).

Detector -1				
Peak Shift	**Integ. CFOV**	**Diff. CFOV**	**Integ. UFOV**	**Diff. UFOV**
0 %	4.67%	1.94%	5.71%	2.89%
1 %	3.68%	2.08%	5.61%	2.86%
2 %	4.44%	2.34%	5.57%	2.57%
3 %	4.49%	2.26%	5.18%	3.08%
4 %	4.65%	2.80%	5.29%	2.84%
5 %	5.19%	3.20%	6.11%	3.38%

Table 11: The calculated values of integral and differential uniformities in CFOV & UFOV for 0%, 1%, 2%, 3%, 4% and 5% peak shift at window width of 25% (Detector 2).

Detector -2				
Peak Shift	**Integ. CFOV**	**Diff. CFOV**	**Integ. UFOV**	**Diff. UFOV**
0 %	8.11%	5.38%	8.34%	5.38%
1 %	8.17%	5.36%	8.92%	5.36%
2 %	7.98%	5.38%	8.91%	5.09%
3 %	8.26%	5.40%	8.86%	5.46%
4 %	8.30%	5.15%	8.66%	5.15%
5 %	8.64%	5.53%	9.12%	5.54%

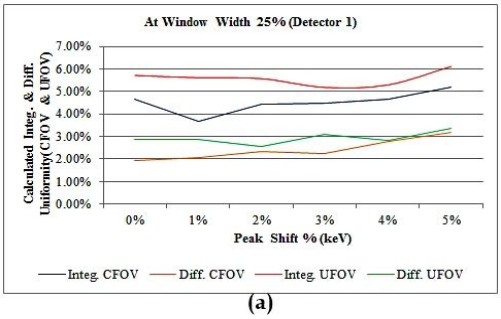

(a)

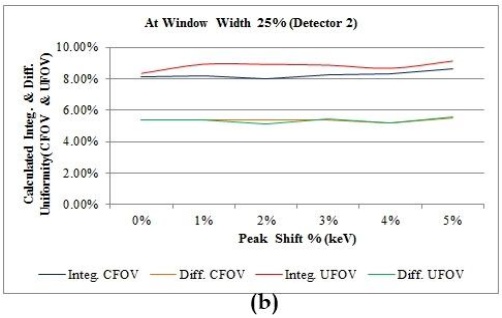

(b)

Fig 6. The calculated integral and differential uniformities in CFOV & UFOV (arbitrary units) versus peak shift percentage (keV) at window width of 25% ((a) Detector 1& (b) Detector 2).

Applied Cases

Thyroid scan: The images of the thyroid taken for the same patient with different peak shifts 0%, 2%, 4% and 6% are shown in Figure 7. The images show a decrease in the overall activity with a loss in the quality of image.

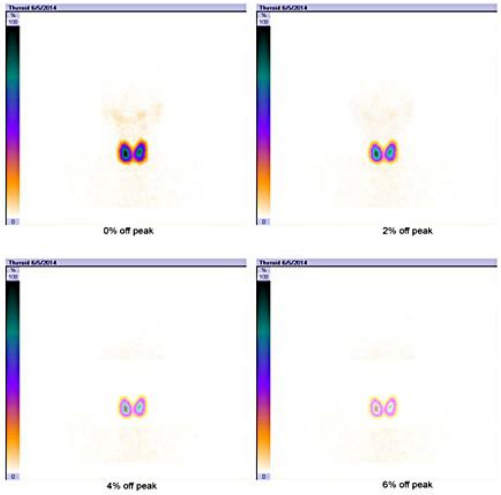

Fig 7. ^{99m}Tc thyroid scan: (1) 0% peak shift(2) 2% peak shift(3) 4% peak shift(4) 6% peak shift.

The first image shows a normal and uniform tracer uptake pattern opposite both Thyroid lobes with no focal lesions i.e. normal morphology and function of the thyroid gland. A decrease in the overall uptake in the salivary glands, thyroid gland and background, with no difference in sintigraphy diagnosis are shown in the second, third and fourth images.

Renal scan: Four images of a kidney scan taken for the same patient with different peak shifts of 0%, 2%, 4% and 6% are given in Figure 8.

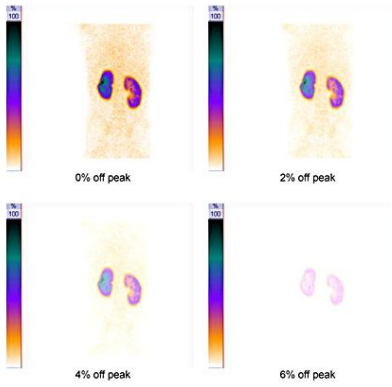

Fig 8. Renal scan: (1) peak shift 0% (2) peak shift2% (3) peak shift 4% (4) peak shift 6%.

Different image quality is shown in the scan, which indicates of change in the tracer distribution in the kidney.

The first image indicates normal (good and uniform tracer uptake pattern with normal cortical portrayal); the second image shows a mild decrease in overall tracer content which indicates of early diffuse parenchyma renal disease. The third image shows a moderate overall decrease in tracer uptake with moderately decrease in overall cortical tubular function. The fourth image shows marked decrease in renal uptake with thin (atrophic) cortex that can be attributed to chronic parenchyma renal disease with marked cortical tubular function loss which leads to a false diagnosis.

SPECT images using heart phantoms: The outer cavity of heart phantom is filled with approximately 1.5 mCi ^{99m}Tc, and then leaves a small residual air bubble.

The peak shift percentage effect on SPECT images using heart phantoms shows four rows of vertical long axis cuts of the heart phantom SPECT study with 4 peak shifts at window width of 15% as shown in Figure 9.

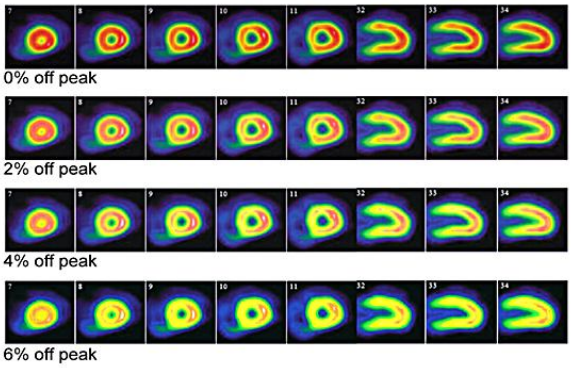

Fig 9. Heart phantom SPECT study: (1) peak shift0% (2) peak shift2% (3) peak shift4% (4) peak shift6% at window width of 15%.

In the first to third rows, there is a single moderate sized perfusion defect that shows marked hypo-perfusion. Images in the fourth row show degraded quality with exaggerated defect (large area of severe hypo-perfusion). In addition, the inferior wall shows rather non-uniform tracer distribution. Nearly the same views and results are repeated in the different off-peaks.

CONCLUSION

The effect of peak shift and window width of energy on SPECT image uniformity is investigated using the calculated integral and differential CFOV and UFOV uniformity values versus the change in both of peak shift and window width. It is evident that energy window width plays a prominent role in flood image uniformity. In conclusion, it can be said that, in planar and SPECT images, the uniformity and quality of images are affected by a change of the peak shift and the effect becomes more pronounced at the peak shift of more than 2%. Thus, Gamma camera used for this purpose is recommended to be operated with peak shifts less than 2% and window width in the range 15% to 20%, otherwise images with bad quality and uniformity will lead to false diagnosis.

REFERENCES

1. Al-Lehyani SHA. Effect of peak shift on planer and SPECT images. J King Saud Univ Sci. 2006:19(1):59-71.
2. Baron JM, Chouraqui P. Myocardial single-photon emission computed tomographic quality assurance. J Nucl Cardiol. 1996 Mar-Apr;3(2):157-66.
3. Groch MW, Erwin WD. SPECT in the year 2000: basic principles. J Nucl Med Technol. 2000 Dec;28(4):233-44.
4. Groch MW, Erwin WD. Single-photon emission computed tomography in the year 2001: instrumentation and quality control. J Nucl Med Technol. 2001 Mar;29(1):12-8.
5. Critchly M. Nuclear Medicine Pocket Handbook. Amersham International PLC;1993. pp. 67.
6. Lecomte R. Biomedical Imaging: SPECT and PET. AIP Conf Proc. 2007;115:958.
7. Kang D, Sung YW, Kang CK. Fast Imaging Technique for fMRI: Consecutive Multishot Echo Planar Imaging Accelerated with GRAPPA Technique. Biomed Res Int. 2015;2015:394213.
8. O'Connor MK. Instrument- and computer-related problems and artifacts in nuclear medicine. Semin Nucl Med. 1996 Oct;26(4):256-77.
9. De Agostini A, Zatta G, Bagliani G, Tarolo GL. Proposal for a quality control procedure for rotating gamma camera tomographic systems. Radiol Med. 1987 Jul-Aug;74(1-2):109-15.
10. Early PJ. Textbook of Nuclear Medicine Technology. 4th ed., Mosby; 1995.
11. Dinish US, Song Z, Ho CJH, Balasundaram G, Attia ABE, Lu X, Tang BZ, Liu B, Olivo M. Single Molecule with Dual Function on Nanogold: Biofunctionalized Construct for In Vivo Photoacoustic Imaging and SERS Biosensing. Adv Funct Mater. 2015;25(15):2316-2325.
12. Evdokimov NM, Clark PM, Flores G, Chai T, Faull KF, Phelps ME, Witte ON, Jung ME. Development of 2-Deoxy-2-[(18)F]fluororibose for positron emission tomography imaging liver function in vivo. J Med Chem. 2015 Jul 23;58(14):5538-47.
13. Cherry SR, Sorenson JA, Phelps ME. Physics in Nuclear Medicine. Philadelphia: Saunders-Elsevier; 2003.

14. Patrick DJ, Hakim M, Ahmed F, El Hakim D, Labbe R, Rubimbura V, Hacquin G, Gaux JC, Auguste M, Mansour H, Pernes JM. Effect of sublingual nitro-glycerine premedication on image analysis of using 256 multidetector computed tomography coronary angiography. OMICS J Radiol. 2014, 3(4):173.

15. Cerqueira MD, Matsuoka D, Ritchie JL, Harp GD. The influence of collimators on SPECT center of rotation measurements: artifact generation and acceptance testing. J Nucl Med. 1988 Aug;29(8):1393-7.

16. Saw CB. Effects of centre-of-rotation shift on contrast and spatial resolution of the SPECT system. Nucl Med Commun. 1986 May;7(5):373-9.

17. Mould RF. Quality control of nuclear medicine instrumentation. IAEA, 1983.

18. Iskandrian AS, Heo J, Askenase A, Segal BL, Helfant RH. Thallium imaging with single photon emission computed tomography. Am Heart J. 1987 Oct;114(4 Pt 1):852-65.

19. Abdelhalim MAK, Rizk RAM, Farag HI, Reda SM. Effect of energy window width on planer and SPECT image uniformity. J King Saud Univ Sci. 2009:21(2):145-150.

20. Liu YH, Sinusas AJ, DeMan P, Zaret BL, Wackers FJ. Quantification of SPECT myocardial perfusion images: methodology and validation of the Yale-CQ method. J Nucl Cardiol. 1999 Mar-Apr;6(2):190-204.